# Towards a bistable vibroacoustic nonlinear absorber: optimum efficiency of a bistable nonlinear energy sink

Islem Bouzid, Renaud Côte, Pierre-Olivier Mattei

Nonlinear Dyn
https://doi.org/10.1007/s11071-024-10572-4

RESEARCH

# Towards a bistable vibroacoustic nonlinear absorber: optimum efficiency of a bistable nonlinear energy sink

**Islem Bouzid · Renaud Côte · Pierre-Olivier Mattei**

Received: 8 July 2024 / Accepted: 27 October 2024


**Abstract** Previous works have demonstrated that an elastic membrane can be coupled to an acoustic system and act as a nonlinear energy sink (NES). In this work we study a new design of a bistable vibroacoustic nonlinear absorber. We use NES membranes and change the characteristics of the membranes from monostable to bistable by changing their linear stiffness. We evaluate the efficiency of the bistable membrane using a numerical approach that allows us to compare the attenuation efficiency of the bistable and monostable NES membranes, and find the optimum stiffness. Then we validate it experimentally. We also present analytical tools and we use them to explain the behavior of the membrane and the specific effects of the bistability property. The numerical approach is applied to different membrane configurations with the same results: bistability can improve the efficiency of a vibroacoustic nonlinear absorber.

**Keywords** VibroAcoustic nonlinear energy sink · Bistable · Energy pumping · Optimization

I. Bouzid
LA2MP, ENIS, Route de la Soukra km 4, 3038 Sfax, Tunisia

I. Bouzid · R. Côte (✉) · P.-O. Mattei
Aix Marseille Univ, CNRS, Centrale Marseille, LMA, Aix-en-Provence, France
e-mail: cote@lma.cnrs-mrs.fr

## 1 Introduction

This work concerns VibroAcoustics Nonlinear Energy Sink (VA NES) absorbers. They are one class of NES among several [1]. VA NES are used for passive noise control in the low-frequency range. These absorbers are characterized by the phenomenon of Energy Pumping (EP), which involves the unidirectional and irreversible transfer of vibratory energy from the structure to be controlled to the nonlinear absorber. This phenomenon is also known as Targeted Energy Transfer (TET).

In the field of Acoustics, the initial experimental demonstration of the EP phenomenon was proposed by Cochelin et al. [2]. In this seminal paper, a nonlinear vibroacoustic passive absorber made of a thin circular viscoelastic membrane was developed. The proposed experimental set-up enabled the control of an acoustic field in the vicinity of the first acoustic mode of a tube open at both ends. The tube was coupled to the NES via a coupling box and excited by a loudspeaker. An improved version of this experimental set-up was developed in Bellet's thesis [3], where the energetic transfer of sound energy from the acoustic medium to the membrane was studied experimentally and numerically. A detailed explanation of the main phenomena observed in the free and harmonic regimes was published in [4]. A simplified two-degree-of-freedom (2-dof) model was developed and validated by comparing numerical calculations with experimental results. In [5], the authors demonstrated that the





Journal: 11071 MS: 10572 TYPESET DISK LE CP Disp.:2024/11/1 Pages: 20 Layout: Medium

use of different membranes mounted in parallel on the coupling box made extended the zone of effectiveness of the EP phenomenon. A second experimental device for acoustic EP was developed by Mariani et al. [6]. This device comprised a membrane from a loudspeaker, which could be precisely adjusted in mass and coupled with the primary acoustic medium to be controlled (in this case, the first acoustic mode of an open tube) through a coupling box. In the aforementioned papers, the NES was coupled to the primary system (PS) by a linear stiffness, whose stiffness could be adjusted by controlling the volume of the coupling box. Shao et al. [7] conducted an analysis of the EP for a configuration in which the NES is directly coupled to the PS. In this configuration, the PS was a parallelepipedic acoustic cavity excited on one of its modes, while the NES was always a mounted membrane on one of the surfaces of this cavity. To extend the finding of Shao et al. [7], Shao [8] studied a system where several acoustic modes of the parallelepipedic cavity were modeled. The experimental setup described in [9] was employed to demonstrate the EP between the cavity and the membrane. These non-linear absorbers are typically characterized by a cubic nonlinear stiffness term and offer effective attenuation terms over a wide range of frequencies. However, they exhibit both activation and deactivation thresholds for EP, beyond which no effective one-way energy transfer is observed. This defines the limitation of these absorbers, which have a limited range of effectiveness, set at high excitation levels.

In the mechanical field, it has been demonstrated that bistable NES has a superior performance to cubic NES as evidenced by the papers [10–14]. In [10] the performance of a traditional cubic NES was enhanced by modifying its monostable property towards a bistable one through the introduction of negative linear and nonlinear stiffness components thereby inducing bistability. It was demonstrated that the modified bistable NES exhibited superior vibration absorption capabilities compared to the traditional cubic NES under transient excitation. The two papers [11] and [12] present a comprehensive numerical and analytical study of the transient dynamics of a linear oscillator coupled to a bistable NES that incorporate negative linear stiffness and positive nonlinear cubic stiffness terms. This work shows significant advantages over other types of NES in terms of EP efficiency and overall energy dissipation rate. In the analytical part, the multiscale method and the concept of limiting phase trajectories were employed. The presence of a 1:3 super-harmonic resonance capture regime in parallel with the main 1:1 resonance capture regime has been shown to result in a strong energy exchange between the PS and the bistable NES. A comprehensive numerical investigation of this system, as presented in reference [12], corroborates the analytical findings. The Hamiltonian and damped dynamics of a bistable NES coupled to a linear oscillator have been studied in [13] using the frequency-energy diagram obtained analytically by the averaging complexification method and numerically by the numerical continuation technique. The wavelet transform was superimposed on this diagram for a comparison between the cubic NES and the bistable NES. It was shown that the bistable NES outperforms the cubic NES due to its ability to immediately diffuse the input energy through multiple resonance captures. In [14], the dynamics under harmonic excitation of a linear oscillator coupled to a bistable NES was studied analytically and verified numerically. The thresholds of these different response regimes have been determined using the asymptotic study and the Melnikov method. The efficiency of the different response regimes of the bistable NES was studied by calculating the dissipated energies and compared with a cubic NES, which has a lower efficiency. An optimum configuration was proposed based on the optimal point between the strongly modulated response and the stable periodic response, where the bistable NES has the highest efficiency.

From an experimental point of view, the bistable NES has been implemented in various fields. In [15], the effectiveness of a bistable device was explored analytically by the harmonic equilibrium method and then experimentally with the aim of providing an opposing force to suppress the vibration of a host structure under harmonic excitation. In [16], a linear system formed of two Euler linear beams coupled to a bistable NES was studied experimentally and numerically. It has been shown that this bistable NES is able to significantly reduce the amplitude of multimodal PS. In [17], a similar mechanical bistable NES based on a deformed beam was used for electromechanical energy harvesting. In [18], the authors proposed an improvement in finite structures based on locally resonant metamaterials by using bistable parts. Yao et al. [19] developed a bistable NES with a buckled beam to suppress the vibrations of an unbalanced rotor system.

Several works have been done on bistable magnetic NESs that are based on magnets' attraction and repul-





Journal: 11071 MS: 10572 TYPESET DISK LE CP Disp.:2024/11/1 Pages: 20 Layout: Medium

sion forces [20–23]. A NES of this type was proposed and tested for structural seismic control in [22,23].

To the best of our knowledge, only one bistable NES solution for noise attenuation in vibroacoustics has been proposed so far by Iurasov et al. [24]. The bistable NES developed and applied in vibroacoustics was presented in [16] in order to improve the acoustic insulation of double partitions.

NES optimization is a constant concern [25,26]. The nonlinear nature of the NES implies caution in optimization results. They are highly dependent on the actual excitation source.

The present article is organized as follows. In the second part, the system under study is described: we present the experimental setup, the corresponding monostable adimensional model and we establish the model for a bistable membrane and the procedure for installing the bistable membrane in the experiment. The third part describes the numerical evaluation approach. The effectiveness of the bistable membrane is demonstrated by presenting the variation of the area under the normalized ridge curve as a function of the linear stiffness. Next, the experimental study is presented to validate this result. Then, we determine the characteristic curves of the tube and the membrane, as well as the conditions of interaction between these two degrees of freedom of the system, which are then used to explain the main results of the study, particularly in the monostable and bistable behavior zones of the membrane. In the seventh part, the numerical evaluation approach is applied to different membrane configurations. The last part concludes this paper.

## 2 Description of the system under study

The device used in this work was inspired by the work of Cochelin et al. [2] and Bellet et al. [4] (see Fig. 1). The nonlinear vibroacoustic absorber proposed in these references consists of a thin circular viscoelastic membrane with radius $R_m$ and thickness $h_m$. This membrane is fixed to a support that allows the radius to be changed and an independently adjustable pre-stress to be imposed on the membrane. This absorber makes it possible to control the acoustic field around the first acoustic mode of a tube open at both ends. The two oscillators are coupled by a coupling box. The primary system (tube) is excited by a sinusoidal acoustic field supplied by a loudspeaker.

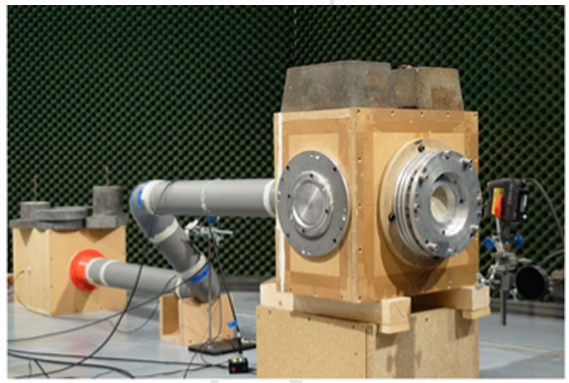

**Fig. 1** Experimental setup

The coupled tube-membrane system's dimensioned model is derived from Bellet's work [4]:

$$u'' + u + \lambda u' + \beta(u - q) = F\cos\left(\frac{\Omega}{\omega_t}\tau\right)$$

$$\gamma q'' + k_l q + k_{nl} q^3 + c_\eta \omega_t \left(2q^2 + 1\right) q' + \beta(q - u) = 0 \quad (1)$$

where $u$ and $q$ are the normalized displacements of the air at the end of the tube and at the center of the membrane, $\lambda$ and $c_\eta\omega_t$ the linear damping coefficients, $2c_\eta\omega_t$ the nonlinear damping coefficient, $\omega_t$ the resonance pulsation of the tube, $F$ the forcing amplitude, $\Omega$ the excitation pulsation, $\beta$ the coupling term, $\gamma$ the dynamic mass, $k_l$ and $k_{nl}$ the linear and cubic stiffnesses of the membrane.

The analytical expressions for the various parameters of this model are presented in [3]. To determine their numerical values, we carry out static and dynamic measurements. Static measurements are used to determine the dimensions of the tube, membrane, and coupling box. This measurement enables us to calculate the stiffness and mass terms. Using a dynamic measurement with a voltage generator and an oscilloscope, we determine the frequencies of maximum amplitude of the pressure in the tube and the displacement of the membrane, as well as the frequency bands at $-3$ dB of these maximum amplitudes. This dynamic measurement, in which the behavior of the system is purely linear, enables us to determine the dissipation terms of the tube and membrane.

In previous works [2,4–9], the NES membrane is a monostable cubic NES. In this paper, we study a bistable NES membrane. The idea behind a bistable membrane is to buckle the membrane, i.e. impose a





Journal: 11071 MS: 10572 TYPESET DISK LE CP Disp.:2024/11/1 Pages: 20 Layout: Medium

buckling pre-stress to obtain a negative linear stiffness. Bistability is achieved by combining cubic stiffness with negative linear stiffness. Subsequently, the model describing the bistable membrane is the same model that describes the monostable membrane, where the linear stiffness value $k_l$ of the membrane is negative.

### 2.1 Bistability condition for the coupled system

The potential energy of the coupled system is expressed as:

$$E_p = \frac{1}{2}k_l q^2 + \frac{1}{4}k_{nl} q^4 + \frac{1}{2}\beta(u-q)^2 + \frac{1}{2}u^2 \qquad (2)$$

By canceling the derivatives of the potential energy with respect to $u$ and $q$, we can determine the static equilibrium positions of the coupled system, which are defined by: $p_0 = (0,0)$, $p_{1,2} = \pm(u_e, q_e)$ where $q_e = \sqrt{\frac{-\beta - k_l(\beta+1)}{k_{nl}(\beta+1)}}$ and $u_e = \frac{\beta}{\beta+1}q_e$. From the second derivative of potential energy, we can deduce that the two equilibrium positions $p_1$ and $p_2$ are stable, while the equilibrium position $p_0$ is unstable.

The linear stiffness is the determining factor for bistability of the system, as determined by the expression of $q_e$ where $-\beta - k_l(\beta+1)$ must be greater than zero. So for this coupled system to have a bistable behavior, the linear stiffness $k_l$ must be less than a critical value $k_{lc} = -\frac{\beta}{\beta+1}$. This critical stiffness value is not zero. This is due to the presence of the coupling term $\beta$, which adds additional stiffness to the linear stiffness of the membrane. It should also be noted that with the presence of this coupling term, the bistability of the membrane influences the behavior of the tube, so that it also exhibits a bistable behavior with two stable equilibrium positions defined by $\pm u_e$.

To sum up, the model Eq. (1) describes the behavior of the monostable system when $k_{lc} > -\frac{\beta}{\beta+1}$ and the behavior of the bistable system when $k_{lc} < -\frac{\beta}{\beta+1}$.

### 2.2 Mounting the NES membrane

To build the bistable NES, we used the same circular viscoelastic membrane as that used to build the monostable NES, but we mounted it differently on its support. In Fig. 2a and b, we have shown the schematic diagram for mounting the monostable membrane and the bistable membrane on the support, respectively. To obtain the monostable NES, the membrane is mounted between the top and bottom rings. Then, by tightening the preload adjustment screws, the assembly of the two rings moved relative to the lower support to stretch the membrane, thus applying a tensile preload to it. In this configuration, the stretching of the membrane ensured that there was a single stable equilibrium position, relative to which the membrane vibrated ($q_e = 0$).

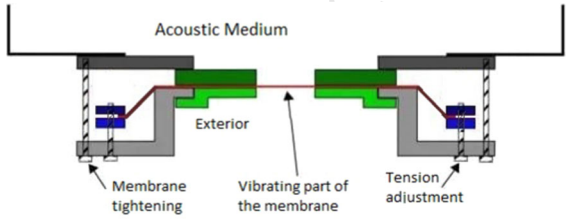


(a) Monostable membrane (Diagram taken from [3]).

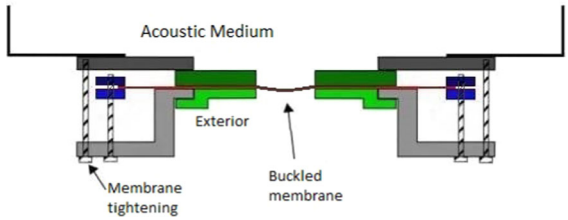


(b) Bistable membrane.

**Fig. 2** Schematic diagram of how the monostable and bistable membranes are mounted on their supports. Dark grey: upper support. Light grey: lower support. Dark green: upper jaw. Light green: lower jaw. Dark blue: upper ring. Light blue: lower ring

To create a bistable membrane, the idea is to buckle the membrane instead of stretching it. To do this, we start by loosening the preload adjustment screws until the lower ring is at the same level as the lower jaw. Then, we place the membrane between the two rings and position a small mass at the center of the membrane to obtain a slight buckling deflection. Next, we secure the membrane between the two rings using fixing screws. During this step, it is important to be careful when tightening these screws to ensure the buckling of the membrane while avoiding the formation of wrinkles. By keeping the mass at the center of the membrane to ensure the presence of buckling, we assemble the lower assembly with the upper assembly. Finally, we remove the mass, thus obtaining a buckled membrane with a deflection $\delta_m$ which constitutes our vibroacoustic nonlinear bistable absorber. The buckling deflection depends on the weight of the mass placed at the center





Journal: 11071 MS: 10572 TYPESET DISK LE CP Disp.:2024/11/1 Pages: 20 Layout: Medium

## 3 Impact of membrane linear stiffness variations on NES performance

### 3.1 Performance criterion definition

In order to know if bistability can improve the absorption efficiency of a membrane NES, we used a numerical approach. This approach is based on the analysis of the ridge curves of the frequency response of the primary system as a function of the linear stiffness of the membrane. Figure 3a shows the response of the primary system coupled to the membrane (air displacement at the end of the tube) as a function of excitation amplitude and frequency. In red, we present the maximum response as a function of the excitation amplitude. The projection of these data onto the (response amplitude, source amplitude) plane shows the tube ridge curves presented in Fig. 3b. This curve is a key tool for understanding the behavior and performance of our system. It explores the behavior over a relatively wide frequency range defined around the tube resonance. Activation and deactivation thresholds of energy pumping are easily identified on this curve. They bound the amplitude range of efficiency of our NES.

The criterion of efficiency used in this study aims at summing up in one number the system behavior over a wide range of source amplitudes and frequencies. We choose here the area below the normalized ridge curve, defined as $\frac{U_{\max}}{F}$ where $U_{\max}$ presents the maximum vibration amplitude of the tube. Figure 4 shows the superposition of two tube ridge curves corresponding to different values of linear stiffness $k_1$ (blue) and $k_2$ (orange). This figure shows that the damping efficiency of the membrane with linear stiffness $k_1$ is larger. This clearly reflects the fact that the ridge curve's area of $k_1$ is smaller than that of $k_2$.

The range of linear stiffness chosen $k_l \in [-0.45, 0.3]$ (i.e. from $-383$ to 255 $\mathrm{N\,m^{-1}}$) includes positive and negative values which make it possible to present the attenuation efficiency of the two types of NES (monostable and bistable) on the same figure, and therefore to compare them easily.

For each value of linear membrane stiffness, the ridge curve is determined numerically. A range of excitation amplitude and frequency is chosen for the calculation. The dimensioned excitation force $F$ varies from 0.01 to 7.5 with 110 steps. The excitation frequency varies around the tube resonance frequency from 70 Hz to 92 Hz with 110 frequency steps. For each excitation amplitude-frequency pair, the time response of air displacement at the end of the tube was determined using the "NDSolve" differential equation numerical solution function defined in Mathematica®. The frequency response was then calculated using the root-mean-square value over the last two seconds of the time signal. For each excitation force, the ridge (maximum) amplitude was determined and normalized (divided) by the excitation amplitude. For each linear stiffness value, the normalized ridge curve is constructed and the area under the ridge curve is calculated.

### 3.2 NES performance assessment

Figure 5 shows the variation of the area under the normalized ridge curves as a function of the linear stiffness of the membrane for a membrane of thickness $h_m = 0.22 \cdot 10^{-3}$ m and radius $R_m = 5 \cdot 10^{-2}$ m. The blue points correspond to monostable behavior, and those in red are related to the bistable system. The broken red line corresponds to the critical value of linear

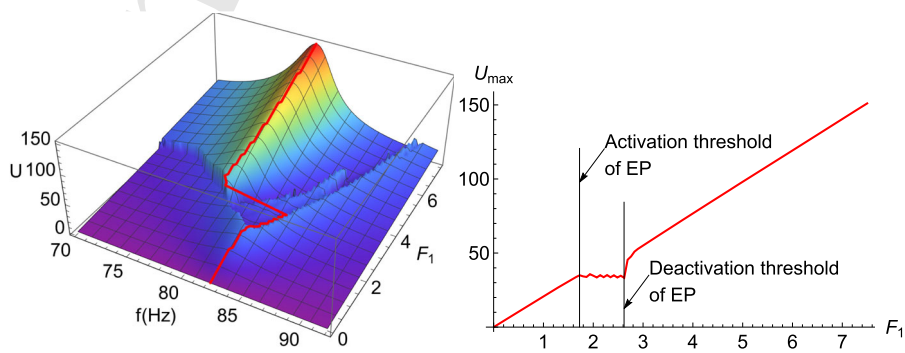


(a) $U(F, f)$ (b) Ridge curve

**Fig. 3** Ridge curve definition. Left: response of the primary system coupled with a membrane as a function of the excitation amplitude and frequency. Right: ridge curve, the projection of the left figure on the (response amplitude, source amplitude) plane





Journal: 11071 MS: 10572 TYPESET DISK LE CP Disp.:2024/11/1 Pages: 20 Layout: Medium

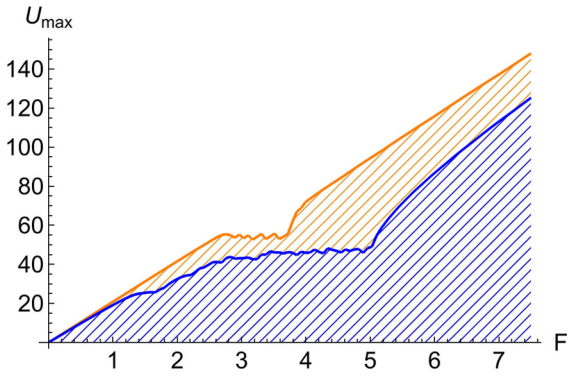


**Fig. 4** Ridge curves for two linear stiffnesses of the membrane. Blue: $k_{l1}$. Orange: $k_{l2}$. The hatched areas highlight their differences

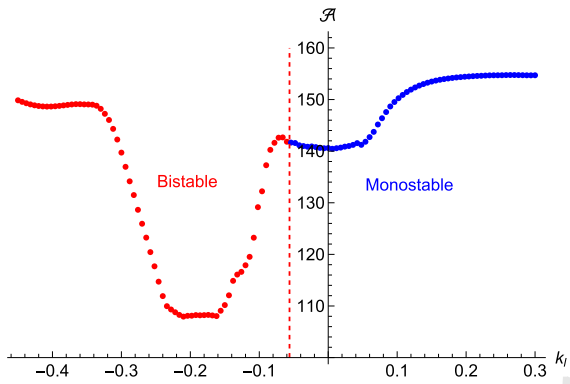


**Fig. 5** Area below normalized ridge curves as a function of the linear stiffness of the membrane. Membrane thickness: $h_m = 0.22 \cdot 10^{-3}$ m, radius: $R_m = 5 \cdot 10^{-2}$ m

stiffness $k_{lc}$ which separates these two different types of behaviors.

The variation of the area as a function of $k_l$ clearly shows that the attenuation is significantly greater with the use of a bistable membrane, since it has smaller area values. In addition, either in the monostable or bistable region, the curve shows an extended minimum plateau over a wide range of linear stiffness. The robustness of this nonlinear absorber (bistable or monostable) is shown by the fact that the minimum is not very pronounced. The membrane parameters are in realistic ranges, which enables experimental checks.

## 4 Experimental validation

In this section we measure the response of the system with different settings of the membrane stiffness, in monostable and bistable state.

As far as the experimental validation is concerned, we follow the same approach as that used in the numerical approach. We explore the overall behavior of the system. The amplitude-frequency excitation range of the voltage sent to the loudspeaker is set at $V \in [0.01, 1.5]$ V and $f \in [70, 92]$ Hz. With 60 frequency steps and 60 amplitude steps, 36 h are required to record the 3600 measurement. Sound pressure measurements are taken in the middle of the tube using a microphone, where it is nearly proportional to the air displacement at the end of the tube [5]. A laser displacement sensor records the displacement of the center of the membrane.

In order to study the effect of the variation of the linear stiffness on the behavior of our coupled tube-membrane system, we choose, in this part, to vary only the pre-stress (buckling or tensile) applied to the membrane, while keeping the diameter and thickness of the membrane constant ($h_m = 0.24$ mm and $R_m = 4$ cm). Seven different configurations of bistable membranes are realized, with buckling varying between 1.9 and 7.2 mm. For comparison, two other monostable membrane configurations are set, with coupled eigenvalues of $f_{m,\text{coupl}} = 64.8$ Hz and $f_{m,\text{coupl}} = 17.5$ Hz.

For bistable membranes, the value of linear stiffness $k_l$ is determined from the equality between the measured buckling $\delta_m$ and the expression of the static equilibrium position $q_e$: $k_l = -\delta_m^2 k_{nl} - \frac{\beta}{\beta+1}$. For monostable membranes, the value of the coupled eigenfrequency of the membrane $f_{mc}$ is measured at very low excitation amplitude, where the nonlinear terms are not effective. The value of the linear stiffness $k_l$ is identified by solving the equation $f_{mc} = f_1$ where $f_1$ presents the expression of the coupled eigenfrequency (later defined in the Eq. (6)).

Table 1 summarizes the buckling, dimensioned linear stiffness and dimensioned linear stiffness for the different bistable membrane configurations:

In Table 2, we present, for the different configurations of monostable membrane, the coupled eigenfrequency of the membrane (since $\delta_m = 0$), the linear stiffness and the dimensioned one.

The second configuration of the monostable membrane in Table 2 has a negative linear stiffness of





Journal: 11071 MS: 10572 TYPESET DISK LE CP Disp.:2024/11/1 Pages: 20 Layout: Medium

**Table 1** The different configurations of bistable membranes

| $\delta_m(m)$ | 0.0019 | 0.004 | 0.0045 | 0.0046 | 0.0059 | 0.0075 | 0.0082 |
|---|---|---|---|---|---|---|---|
| $k_l$ | −0.077 | −0.15 | −0.17 | −0.18 | −0.25 | −0.38 | −0.44 |
| $c_l$ (N.m$^{-1}$) | −26.8 | −52.2 | −59.2 | −62.7 | −87.1 | −132.4 | −153.3 |

**Table 2** The different configurations of monostable membranes

| $f_m$ (Hz) | 64.8 | 17.5 |
|---|---|---|
| $k_l$ | 0.14 | −0.042 |
| $c_l$(N.m$^{-1}$) | 48.8 | −14.6 |

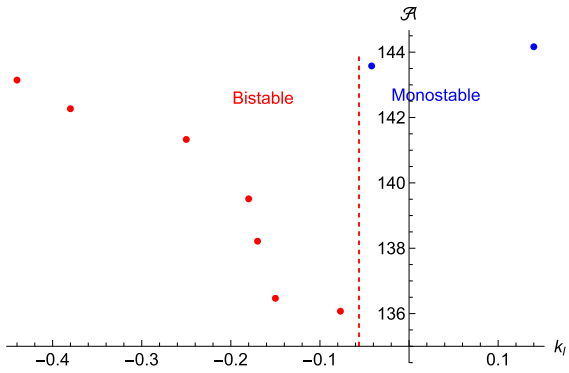


**Fig. 6** The variation of the area under the ridge curves as a function of the linear stiffness of the membrane, determined experimentally

$k_l = -0.042$. This stiffness value is greater than the critical buckling value, which is −0.056.

From the experimental recordings we get the frequency responses of the air displacement at the end of the tube and then the normalized ridge curves and their areas. Figure 6 shows the variation in area determined experimentally. Comparison of this curve with the numerically determined curve shows that we observe similar trends.

So far, we have demonstrated that a bistable membrane improves the performance of a vibroacoustic NES. We have proven this result experimentally. In the following, we want to find the reason of this enhanced performance. To do this, we use theoretical tools for a deeper analysis of the model.

## 5 Tools for theoretical analysis

This part presents the theoretical tools used later for the analysis of the system behavior. Although presented comprehensively, they are very simple because based on the uncoupled elements of the system or on linear analysis. Nevertheless, they give the key information about the various behaviors of the system.

### 5.1 Characteristic curves

We determine here the characteristic curve of the monostable and bistable membranes and the tube. These curves show the variation of the natural frequency as a function of vibration amplitude. These curves show the characteristics of each oscillator alone. The coupling between the two oscillators is not taken into account.

To approximate the effective system, we assume that the stiffness term $\beta$ acts as an additional linear stiffness added to the membrane stiffness $k_l$. The equation governing the free vibrational motion of the uncoupled membrane is defined by $\gamma q'' + (k_l + \beta)\, q + k_{nl} q^3 = 0$. We introduce the expression $q(\tau) = A\cos\omega\tau$ into this equation, where $A$ represents the vibration amplitude of the membrane. The harmonic balance method is applied and the higher order harmonics are suppressed. The following equation is obtained: $-\gamma\omega^2 + k_l + \beta + 3/4 k_{nl} A^2 = 0$. Therefore, the square of the resonance pulsation is defined as $\omega^2 = \frac{|k_l+\beta+\frac{3}{4}k_{nl}A^2|}{\gamma}$. For the monostable membrane, where $k_l > 0$, this pulsation is defined by $\omega = \sqrt{\frac{k_l+\beta+\frac{3}{4}k_{nl}A^2}{\gamma}}$. For the bistable membrane, where $k_l < 0$, the pulsation depends on the amplitude of vibration $A$. More precisely, it is equal to $\omega = \sqrt{\frac{-k_l-\beta-\frac{3}{4}k_{nl}A^2}{\gamma}}$ if $A < \sqrt{\frac{-k_l-\beta}{\frac{3}{4}k_{nl}}}$, and to $\omega = \sqrt{\frac{k_l+\beta+\frac{3}{4}k_{nl}A^2}{\gamma}}$ if $A > \sqrt{\frac{-k_l-\beta}{\frac{3}{4}k_{nl}}}$. Similarly, for the tube, by introducing the expression $u(\tau) = B\cos\omega\tau$ into the





Journal: 11071 MS: 10572 TYPESET DISK LE CP Disp.:2024/11/1 Pages: 20 Layout: Medium

equation describing its behavior $u'' + u + \beta u = 0$ and applying the harmonic balance method, the expression for the scaled pulsation is determined. The pulsation is equal to $\sqrt{1+\beta}$ whatever the value of the amplitude $B$.

Figures 7a and b show respectively the superposition of the characteristic curves of a monostable and bistable membrane with that of the tube. The characteristic curve for the tube, shown in red, is linear, and the resonance frequency is independent of the vibration amplitude. In the case of the monostable membrane, the resonance frequency increases as the vibration amplitude increases. In this case, the characteristic curve shows a stiffening behavior. For the bistable membrane, the characteristic curve shows two types of behavior. A softening behavior is observed at low vibration amplitude, in which the resonance frequency decreases with increasing amplitude. When this frequency becomes equal to zero, the behavior becomes stiffening (the frequency increases). These curves provide an indication of the presence of resonance capture between the two oscillators, easily identifiable by the intersection between the characteristic curves of the tube and the membrane. As energy is injected into the system, the resonance frequency of the membrane will follow this characteristic curve until it reaches the resonance frequency of the tube, leading to resonance capture where the energy pumping phenomenon takes place.

In Fig. 8a and b, the characteristic curves of a monostable and bistable membrane are superimposed on those of the tube, respectively, when the natural frequency (observed at low vibration amplitude) of the membrane is higher than that of the tube when the natural frequency of the membrane is lower than that of the tube. For the monostable membrane, the characteristic curves show no common point. In this case, there is no resonance capture between the two oscillators. On the other hand, for the bistable membrane, when its natural frequency becomes higher than that of the tube, the characteristic curves show two points of intersection. In this case, there are two resonance captures.

## 5.2 Linearized coupled system

Analysis of the characteristic curves highlights the fundamental difference in the behavior of the system observed in the two cases when the natural frequency of

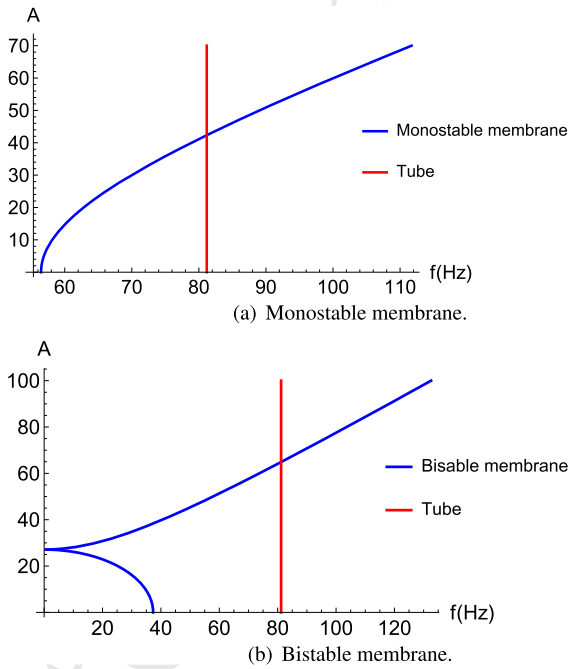


(a) Monostable membrane.

(b) Bistable membrane.

**Fig. 7** Characteristic curves (amplitude versus natural frequency) of the monostable (**a**) and bistable (**b**) membrane with that of the tube when the natural frequency of the membrane is lower than that of the tube

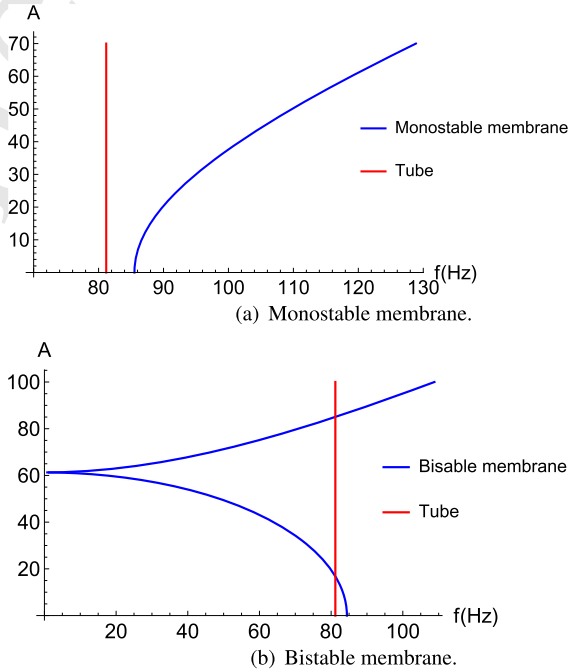


(a) Monostable membrane.

(b) Bistable membrane.

**Fig. 8** Characteristic curves of the monostable (**a**) and bistable (**b**) membrane with that of the tube when the natural frequency of the membrane is higher than that of the tube



Journal: 11071 MS: 10572 TYPESET DISK LE CP Disp.:2024/11/1 Pages: 20 Layout: Medium

the membrane is higher or lower than that of the tube. In this section, we take the coupling into account. The coupling is small, so the coordinates of the degrees of freedom of the system remain close to the tube and membrane displacements. The coordinates of the degrees of freedom of the system are given by the eigenvectors of the modal analysis of the linearized model. We study the variation of the natural frequencies of the coupled system as a function of the linear stiffness of the membrane in order to determine the monostable and bistable situations, and to attribute the proper degree of freedom to the eigenfrequencies.

For the bistable system, the position $p_0$ corresponds to the point of unstable equilibrium. To capture the dynamics of the small-amplitude system, it is more convenient to rewrite the equations in terms of $x = u - u_e$ and $x = u - u_e$ and $y = q - q_e$ so that $(x, y) = (0, 0)$ corresponds to a stable equilibrium position. The system Eq. (1) is rewritten as follows.

$$\begin{aligned} & x'' + x + \lambda x' + \beta(x - y) = F\cos\left(\frac{\tau\Omega}{\omega_t}\right) \\ & \gamma y'' + c_\eta \omega_t \left(2q_e^2 + 4q_e y + 2y^2 + 1\right) y' \\ & + y\left(k_l + 3k_{nl}q_e^2\right) + 3k_{nl}q_e y^2 + k_{nl}y^3 \\ & + \beta(y - x) = 0 \end{aligned} \tag{3}$$

To determine the expressions of the natural frequencies of this bistable system, it must be reduced to an undamped free linear system. By eliminating the nonlinear, forcing and damping terms, the resulting system of equations is rewritten in this matrix form

$$\begin{aligned} & MX'' + KX = 0 \\ & M = \begin{pmatrix} 1 & 0 \\ 0 & \gamma \end{pmatrix}, K = \begin{pmatrix} \beta + 1 & -\beta \\ -\beta & \frac{3\beta^2}{\beta+1} - 2\beta + k_l \end{pmatrix}, \\ & X = \begin{pmatrix} x \\ y \end{pmatrix} \end{aligned} \tag{4}$$

$M$ and $K$ are the mass and linear stiffness matrices. The coupled eigenfrequencies are determined by calculating the eigenvalues of the linear system Eq. (4). They have the following expressions:

$$\begin{aligned} f_1 &= \frac{\omega_t}{2\pi}\sqrt{\frac{f_\alpha - \sqrt{f_\alpha^2 + 8\gamma(\beta + \beta k_l + k_l)}}{2\gamma}} \\ f_2 &= \frac{\omega_t}{2\pi}\sqrt{\frac{f_\alpha + \sqrt{f_\alpha^2 + 8\gamma(\beta + \beta k_l + k_l)}}{2\gamma}} \end{aligned} \tag{5}$$

where $f_\alpha = \frac{3\beta^2}{\beta+1} + \beta(\gamma - 2) + \gamma - 2k_l$. These frequencies are valid for the bistable system when $k_l$ is less than the critical value $k_{lc}$. When $k_l$ becomes greater than $k_{lc}$, the behavior becomes monostable. The same calculation steps carried out previously are applied to the monostable system model to determine these natural frequencies:

$$\begin{aligned} f_1 &= \frac{\omega_t}{2\pi}\sqrt{\frac{\beta\gamma + \beta + \gamma + k_l - \sqrt{(\beta\gamma + \beta + \gamma + k_l)^2 - 4\gamma(\beta + \beta k_l + k_l)}}{2\gamma}} \\ f_2 &= \frac{\omega_t}{2\pi}\sqrt{\frac{\beta\gamma + \beta + \gamma + k_l + \sqrt{(\beta\gamma + \beta + \gamma + k_l)^2 - 4\gamma(\beta + \beta k_l + k_l)}}{2\gamma}} \end{aligned} \tag{6}$$

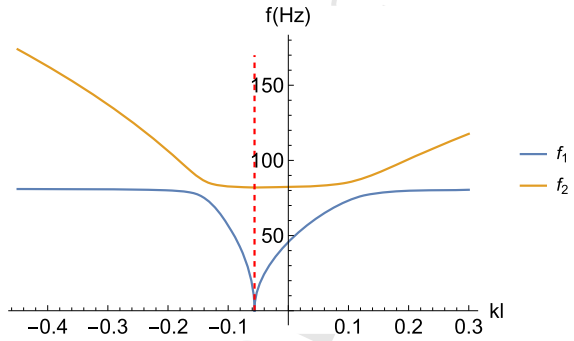


**Fig. 9** Coupled system eigenvalues $f_1$ and $f_2$ as a function of the membrane stiffness. The discontinuous red line corresponds to the critical linear stiffness value $k_{lc}$ that separates the monostable and bistable zones

Figure 9 shows the variation of these two frequencies as a function of linear stiffness for the membrane with $h_m = 0.22$ mm and $R_m = 50$ cm. The selected dimensioned linear stiffness varies between $-0.45$ and 0.3. Is shows natural frequencies of the coupled tube-membrane system in monostable and bistable mode. The dashed red line shows the linear stiffness value $k_{lc}$ which separates the monostable zone from the bistable zone.





Journal: 11071 MS: 10572 TYPESET DISK LE CP Disp.:2024/11/1 Pages: 20 Layout: Medium

Each of the natural frequencies $f_1$ and $f_2$ corresponds to one of the two degrees of freedom of this system. For example, for the monostable behavior at $k_{lc}$, the frequency $f_1$ is equal to zero. It corresponds to the natural frequency of the membrane and $f_1$ corresponds to the natural frequency of the tube. With the increase of the value of linear stiffness, the natural frequency of the membrane increases, while that of the tube follows the horizontal asymptote $f = 82$ Hz. At linear stiffness $k_{l1}$, the natural frequency of the membrane becomes higher than that of the tube. The frequency $f_2$ corresponds to the membrane and $f_1$ to the tube. This frequency exchange is also observed during bistable behavior when the linear stiffness reaches a certain value $k_{l2}$. The frequency exchange is visible through the parallel straight lines normal to the curves representing the functions $f_1$ and $f_2$. The equation of the straight line normal to the curve representing $f_i$ at the point with abscissa $k_l$ is defined by: $N_i(K_L, k_l) = \frac{-1}{f_i'(k_l)}(K_L - k_l) + f_i(k_l)$ $(i = 1; 2)$. The linear stiffness $K_L$ represents the axis of abscissa which defines the domain of definition of the function $N_i$, while the corresponding stiffness $K_l$ is the point from which we determine the equation of the normal line. In order for two regular lines to be parallel, the distance between them must be equal. So, to determine the values of linear stiffness $k_{l1}$ and $k_{l2}$ for which the natural frequency of the membrane becomes greater than that of the tube, it is necessary to solve the equations $N_1(0, k_{l1}) - N_2(0, k_{l1}) = N_1(0.1, k_{l1}) - N_2(0.1, k_{l1})$ and $N_1(0, k_{l2}) - N_2(0, k_{l2}) = N_1(0.1, k_{l2}) - N_2(0.1, k_{l2})$. The choice of the values $K_L = 0$ and $K_L = 0.1$ used for the resolution is random; any values can be chosen.

Figure 10 shows in blue the natural frequency of the tube (in red) ad of the membrane (in blue) as a function of the linear stiffness. The discontinuity points of these two curves are at the linear stiffnesses $k_{l1}$ and $k_{l2}$. The normals to the curves representing the functions $f_1$ and $f_2$ at the abscissa points $k_{l1}$ and $k_{l2}$ are shown by the parallel lines in green. The discontinuous red line is the critical linear stiffness value $k_{lc}$.

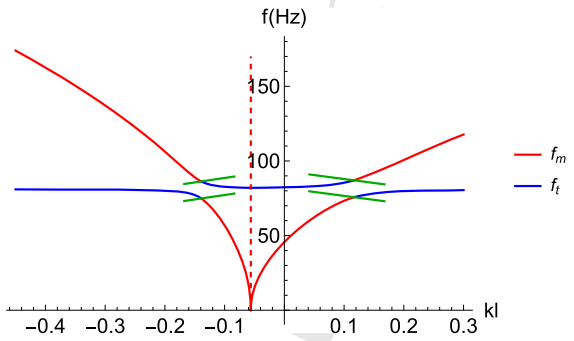


**Fig. 10** Coupled natural frequencies of the tube $f_t$ (blue) and membrane $f_m$ (red) as a function of the linear stiffness of the membrane. The discontinuous red line corresponding to the critical linear stiffness value $k_{lc}$ that separates the monostable and bistable zones. The green parallel lines, present the normals to the representative curves of functions $f_1$ and $f_2$, from which the natural frequency of the membrane becomes higher than that of the tube

## 6 Analysis of the system behavior

We analyze here the behavior of the system in the different zones of the normalized ridge curve area versus stiffness curve.

When the value of the linear stiffness is increased further, the frequency of the coupled membrane becomes higher than that of the tube. Resonance capture between the two oscillators is no longer possible (there is no point of intersection in the characteristic curves). The membrane becomes inactive, the behavior of the system becomes linear (see Fig. 15) and the ridge curves show a straight line. In this zone, there is no more energy pumping.

### 6.1 Monostable behavior

The monostable behavior is analyzed in three distinct zones: optimal behavior zone, non-optimal behavior zone where $f_m < f_t$, and beyond optimal behavior zone where $f_m > f_t$. Figures 11, 13 and 14 show respectively, for each of these zones, the tools used to explain the behavior of the system.

- Figure (a), top left, shows the area as a function of linear stiffness is shown by circling the relevant zone. The dashed red line corresponds to the critical linear stiffness value $k_{lc}$. The green dashed lines delimit the zone where the natural frequency of the tube is greater than that of the membrane.
- Figure (b), top right, shows the superposition of the different ridge curves.
- Figure (c), bottom, the various characteristic curves of the monostable membrane are superimposed on those of the tube.





Journal: 11071 MS: 10572 TYPESET DISK LE CP Disp.:2024/11/1 Pages: 20 Layout: Medium

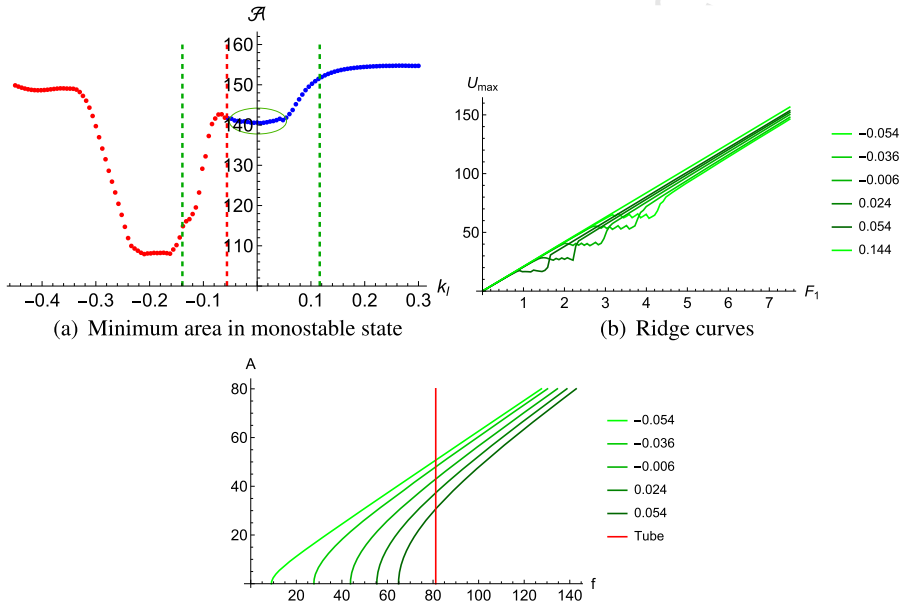


(a) Minimum area in monostable state

(b) Ridge curves

(c) Characteristic curves: membrane (green), tube (red).

**Fig. 11** Behavior and state of the system in the optimal monostable zone

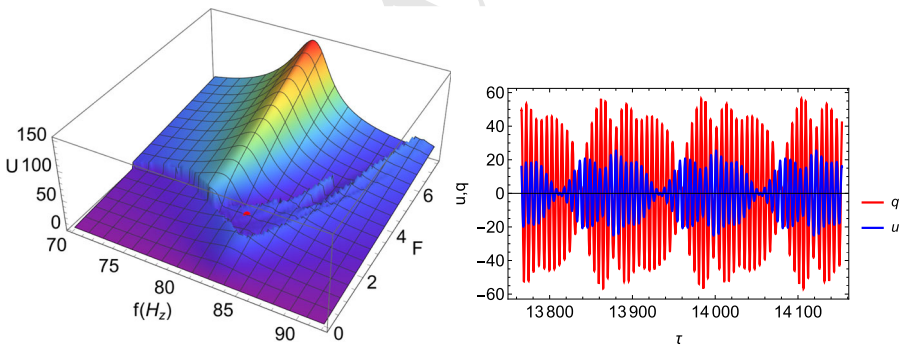


(a) $U(f,F)$.

(b) Time response for $F = 2.34$ and $f = 81.9$ Hz.

**Fig. 12** Numerical simulation result for $k_l = 0.024$. **a** Response of the primary system as a function of excitation amplitude and frequency. **b** Excerpt of the steady state time response of the system for the red point in (**a**)

In these figures, a different shade of color is used for each zone (optimal behavior: green, beyond optimal behavior where $f_m > f_t$: orange and when $f_m > f_t$: discontinuous red).

First, we look at the zone of optimum behavior for the monostable system. This zone is observed when the natural frequency of the tube is higher than that of the membrane. In this zone, the characteristic curves always show a resonance capture between the tube and the membrane, the amplitude of intersection of which increases as the linear stiffness value decreases. Energy pumping is therefore always observed, and it appears at increasingly higher amplitudes. This can be seen in the ridge curves. In this zone, we can see that as the linear stiffness value decreases, the energy pumping activation threshold becomes higher and the plateau deeper. In this zone, we have the same value of the area, even though the activation threshold and the width of the EP plateau are not similar for the different linear stiffness values. In this case, there is a compromise between the level of appearance and the depth of the energy pumping plateau.

Figure 12 shows the result of the numerical simulation. The response of the primary system as a function of excitation amplitude and frequency is shown in Fig. 12a. This 3D figure shows the different regimes of behavior of the usual nonlinear system, a linear behavior at low excitation level with a straight resonance ridge corresponding to the tube natural frequency, then we observe the clipping of the tube resonance peak,



Journal: 11071 MS: 10572 TYPESET DISK LE CP Disp.:2024/11/1 Pages: 20 Layout: Medium

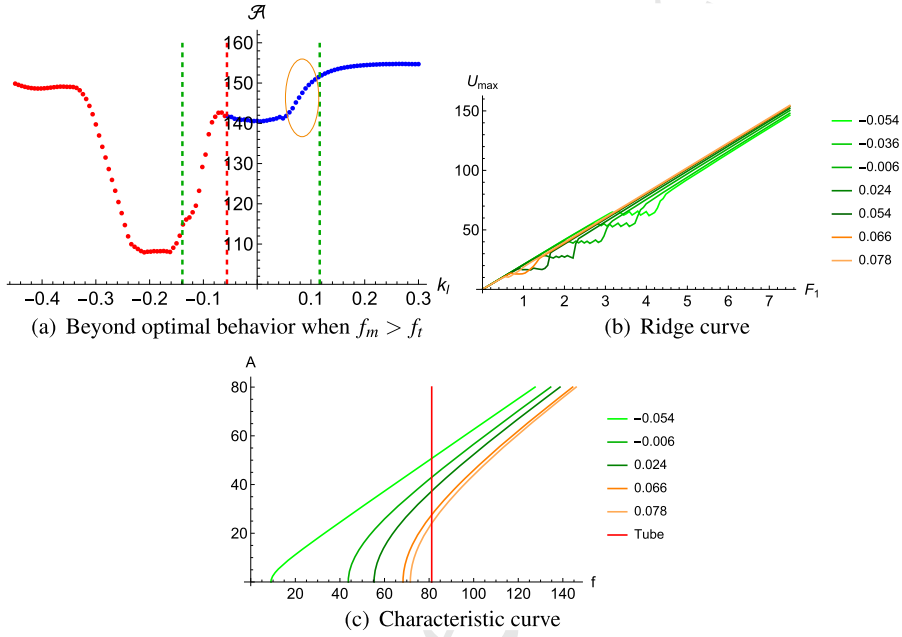


**Fig. 13** Behavior and state of the system beyond optimal behavior, with $f_m < f_t$

(a) Beyond optimal behavior when $f_m > f_t$

(b) Ridge curve

(c) Characteristic curve

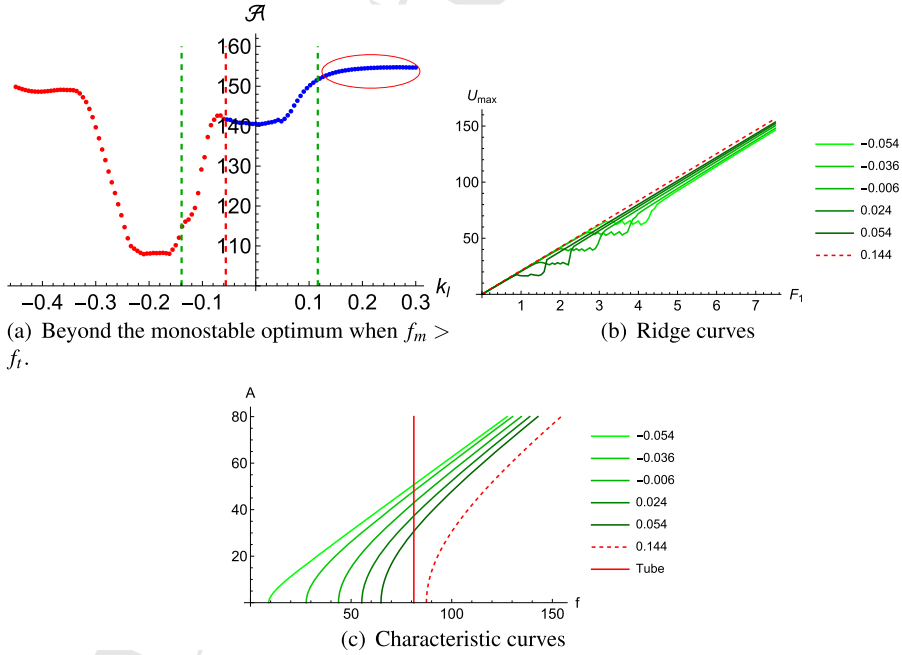


**Fig. 14** System behavior and state beyond the optimal monostable zone, with $f_m > f_t$

(a) Beyond the monostable optimum when $f_m > f_t$.

(b) Ridge curves

(c) Characteristic curves

which corresponds to the energy pumping zone. The time response of the system corresponding to the red point in this zone is shown in the sub-figure Fig. 12b. It shows the strongly modulated response that characterizes energy pumping. If the excitation amplitude is increased further, a new resonance ridge appears, shifted slightly towards the low frequencies.

As the linear stiffness value increases, the optimum behavior zone is left. Resonance capture is still possible with smaller amplitudes. The ridge curves show that the activation threshold becomes weaker, but the plateau becomes very narrow. In this zone, the low activation level of energy pumping cannot compensate for the small extension of the pumping plateau, so the system leaves the optimum zone.



Journal: 11071 MS: 10572 TYPESET DISK LE CP Disp.:2024/11/1 Pages: 20 Layout: Medium

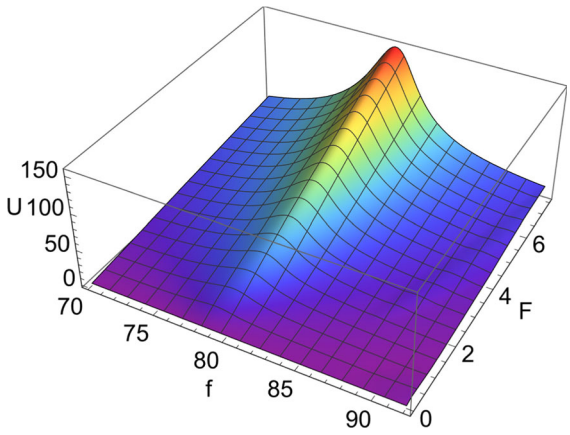


**Fig. 15** The numerical simulation result for $k_l = 0.144$: response of the primary system as a function of excitation amplitude and frequency

## 6.2 Bistable behavior

For linear stiffness values below the critical value $k_{lc}$, the apparent linear stiffness of the membrane becomes negative, and the system's behavior becomes bistable. In this section, we study the system's behavior in three zones: when the natural frequency of the membrane is lower than that of the tube, when the natural frequency of the membrane becomes higher than that of the tube in the optimal behavior zone, and beyond the optimal behavior zone. Figures 16, 18, and 20 correspond to these three zones, respectively. In these figures, we present, as in the previous section, the area in the concerned zone, as well as the ridge curves and characteristic curves.

First, let's focus on the bistable behavior zone when the natural frequency of the membrane is lower than that of the tube. For the initial stiffness values that are below $k_{lc}$, our system exhibits a transitional zone for the shift from monostable to bistable behavior. A "purely" bistable behavior is observed from the linear stiffness value $k_l = -0.12$. In subfigure Fig. 16b, we have shown the superposition of several ridge curves for different linear stiffness values, ranging from $[-0.042, -0.12]$. The two green ridge curves correspond to linear stiffness values greater than $k_{lc}$, thus corresponding to monostable behavior. The other ridge curves correspond to an apparent linear stiffness less than zero. For the initial linear stiffness values that are lower than the critical value $k_{lc}$, the continuous black ridge curves ($k_l = -0.066$ and $k_l = -0.072$) show a continuity of behavior. The behavior observed for the bistable system follows the variation of the monostable system. With the decrease in linear stiffness, it was noticed that the variation of the ridge curves presented in gray shows the presence of an energy pumping plateau at the same level as that observed for $k_l = -0.12$, followed by an increase in vibration amplitude that follows the variation of the monostable ridge curves. At the linear stiffness $k_l = -0.12$, the



**Fig. 16** System behavior and state in the bistable zone whith $f_m < f_t$

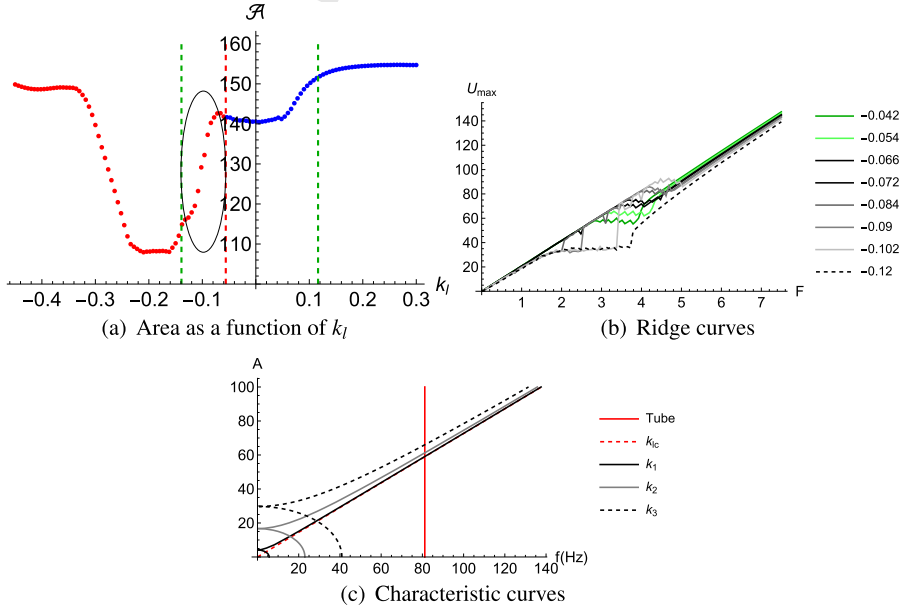


(a) Area as a function of $k_l$

(b) Ridge curves

(c) Characteristic curves



Journal: 11071 MS: 10572 TYPESET DISK LE CP Disp.:2024/11/1 Pages: 20 Layout: Medium

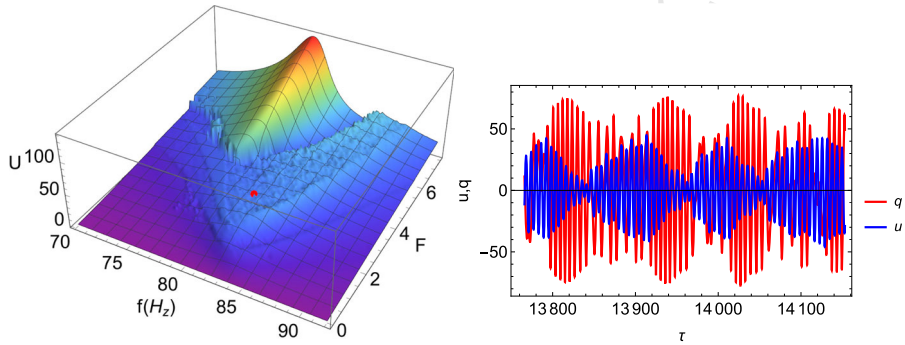


(a) $U(f,F)$. (b) Time response for $F = 2.68$ and $f = 81.7$ Hz.

**Fig. 17** Numerical simulation result for $k_l = -0.12$. **a** Response of the primary system as a function of excitation amplitude and frequency. **b** Time response of the system corresponding to the red point in (**a**)

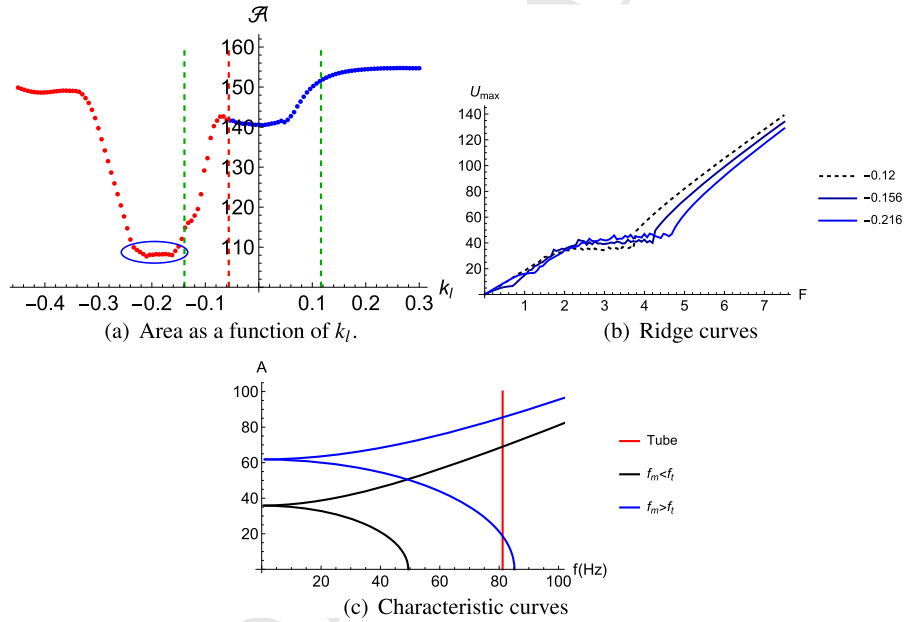


(a) Area as a function of $k_l$. (b) Ridge curves

(c) Characteristic curves

**Fig. 18** Behavior and state of the system in the optimal bistable zone

system stabilizes on the bistable behavior. To transition from monostable behavior (green curves) to bistable behavior (discontinuous black curve), we pass through a transitional zone where the system exhibits both types of behavior. We have a gradual transition.

Figure 16c presents the superposition of three different characteristic curves of a bistable membrane (with linear stiffnesses $k_1$, $k_2$, and $k_3$ where $k_3 < k_2 < k_1$) with the characteristic curve of the tube (red) and the characteristic curve of a purely cubic membrane (discontinuous red). For the black curve, the linear stiffness $k_1$ is very close to the value $k_{lc}$. The softening effect of the bistable membrane is neglected in this case. The characteristic curve overlaps with the discontinuous red curve of the purely cubic membrane. This explains why the system follows monostable behavior for the values $k_l = -0.066$ and $k_l = -0.072$. With the decrease in the linear stiffness value ($k_2$), we move away from the critical value $k_{lc}$. The characteristic curve of the bistable membrane moves away from the discontinuous red curve. The system is influenced by both bistable and monostable behaviors. As the stiffness decreases further ($k_3$), the characteristic curve of the bistable membrane moves further away from the discontinuous red curve. In this case, the system stays on bistable behavior.

In Fig. 17, we present numerical simulation results for the linear stiffness value $k_l = -0.12$. On the left, we present the displacement variation of the tube as a function of amplitude and excitation frequency. On the right, we present the temporal response of the system in the energy pumping zone (for $F = 2.68$ and $f =$



Journal: 11071 MS: 10572 TYPESET DISK LE CP Disp.:2024/11/1 Pages: 20 Layout: Medium

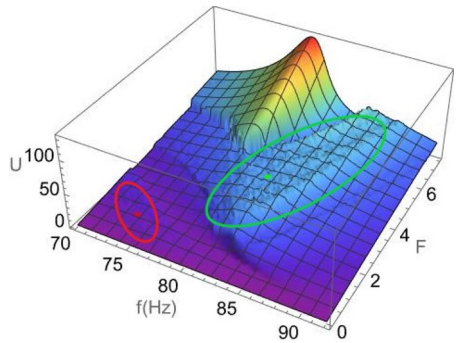


(a) $U(f,F)$

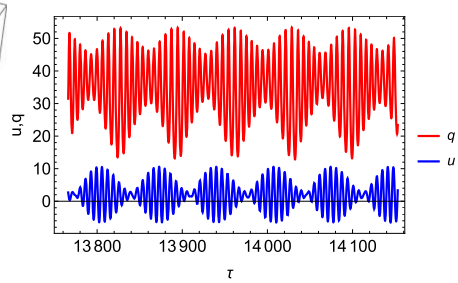


(b) System dynamics for $F = 0.97$ and $f = 73.8$ Hz.

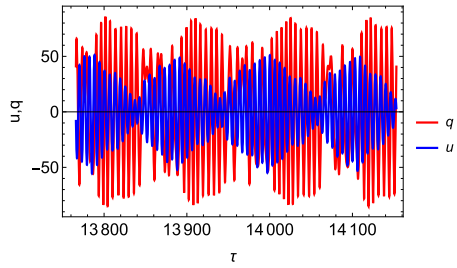


(c) System dynamics for $F = 3.38$ and $f = 81.9\ H$Hz.

**Fig. 19** Numerical simulation result for $k_l = -0.156$. **a** Response of the primary system as a function of excitation amplitude and frequency. **b** Time response of the system corresponding to the red point in this figure (**a**, **b**). **c** Time response of the system corresponding to the green point in (**a**)

81.7 Hz ). This response corresponds to the strongly modulated chaotic regime, which is often observed for bistable systems [14,24].

As the linear stiffness value increases further, the natural frequency of the membrane becomes higher than that of the tube. The zone of optimal behavior is observed. In this zone, the ridge curves exhibit two attenuation plateaus. A narrow plateau is observed at low excitation amplitudes, and the other, broader one is observed at a higher excitation level. The overlap of the characteristic curve of the tube and the bistable membrane shows the presence of two intersection points where both oscillators enter resonance capture, and energy pumping is activated.

In Fig. 19, we present numerical simulation results for the linear stiffness value $k_l = -0.156$. In Fig. 19a, we present the response of the tube as a function of excitation frequency and amplitude. The encircled zones on this figure represent two different energy pumping zones. The time response of the system corresponding to the red ($f = 73.8$ Hz and $F = 0.97$) and green ($f = 81.9$ Hz and $F = 3.38$) points presented in these energy pumping zones is shown respectively Fig. 19b and c. The energy pumping zone observed at low excitation amplitude is characterized by the presence of strongly modulated intrawell response. The second zone is characterized by the presence of strongly modulated chaotic interwell response.

When the natural frequency of the membrane becomes greater than that of the tube, the characteristic curve shows the presence of two resonance captures. The first is observed at low vibration amplitudes, related to the softening behavior of the membrane. This softening resonance capture leads to the presence of energy pumping phenomenon at low excitation amplitudes, characterized by the presence of strongly modulated intrawell response. The second resonance capture, observed at higher amplitudes, is related to the intersection with the stiffening behavior of the membrane. This explains the presence of the second energy pumping zone, characterized by the presence of strongly modulated chaotic interwell response.

As the linear stiffness value is decreased further, we leave the optimal bistable behavior zone (see Fig. 20a). In this range of linear stiffnesses, the ridge curves show the presence of a single high-amplitude energy pumping plateau. We notice the absence of the small pumping plateau that was observed at low vibration levels in the optimal behavior zone.





Journal: 11071 MS: 10572 TYPESET DISK LE CP Disp.:2024/11/1 Pages: 20 Layout: Medium

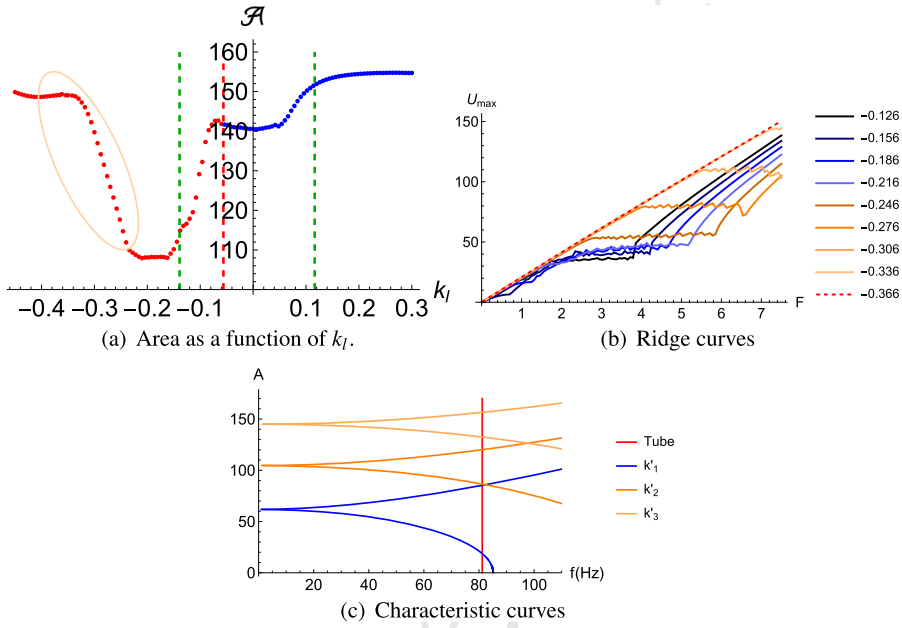


(a) Area as a function of $k_l$. (b) Ridge curves

(c) Characteristic curves

**Fig. 20** Behavior and state of the bistable system beyond the optimal behavior zone with $f_m > f_t$

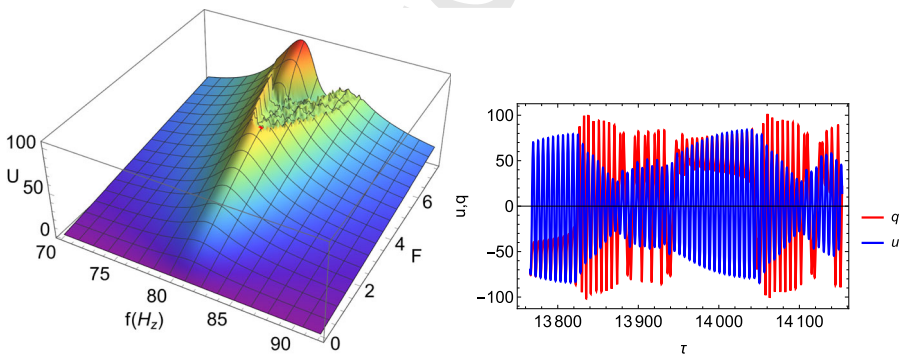


(a) $U(f,F)$ (b) Time response for $f = 80.2$ Hz and $F = 4.4$.

**Fig. 21** Numerical simulation result for $k_l = -0.276$. (a) Response of the primary system as a function of excitation amplitude and frequency. (b) Time response of the system corresponding to the red point in this figure (**a**, **b**)

In Fig. 21, the results of the temporal simulation for a linear stiffness value belonging to this zone are presented ($k_l = -0.276$). The tube response as a function of amplitude and excitation frequency shows the presence of a single energy pumping zone. The temporal response of the system corresponding to the red point indicated in the energy pumping zone (for $f = 80.2$ Hz and $F = 4.4$) is presented in Fig. 21b. This response is different from what we observed before. In Fig. 22a and b, we present respectively for the tube and the membrane the time response (top) and the corresponding wavelet transform (bottom). In these figures, the solid red line corresponds to the natural frequency of the tube and the dashed red line corresponds to the natural frequency of the membrane. The membrane displacement response clearly shows the presence of three different operating regimes:

- Chaotic regime: the system oscillates randomly between the two equilibrium positions.
- Intrawell regime: the system oscillates around one of the equilibrium positions.
- Strongly modulated "interwell" regime: there is resonance capture between the tube and the membrane, resulting in vibrations at the same frequency.

In Fig. 20c, we present the superposition of three different characteristic curves of a bistable membrane (with linear stiffnesses $k_1'$, $k_2'$, and $k_3'$ where $k_3' < k_2' < k_1'$), along with the characteristic curve of the tube (in red), in the case where the natural frequency of the membrane is higher than that of the tube. With the significant decrease in the linear stiffness of the membrane,



Journal: 11071 MS: 10572 TYPESET DISK LE CP Disp.:2024/11/1 Pages: 20 Layout: Medium

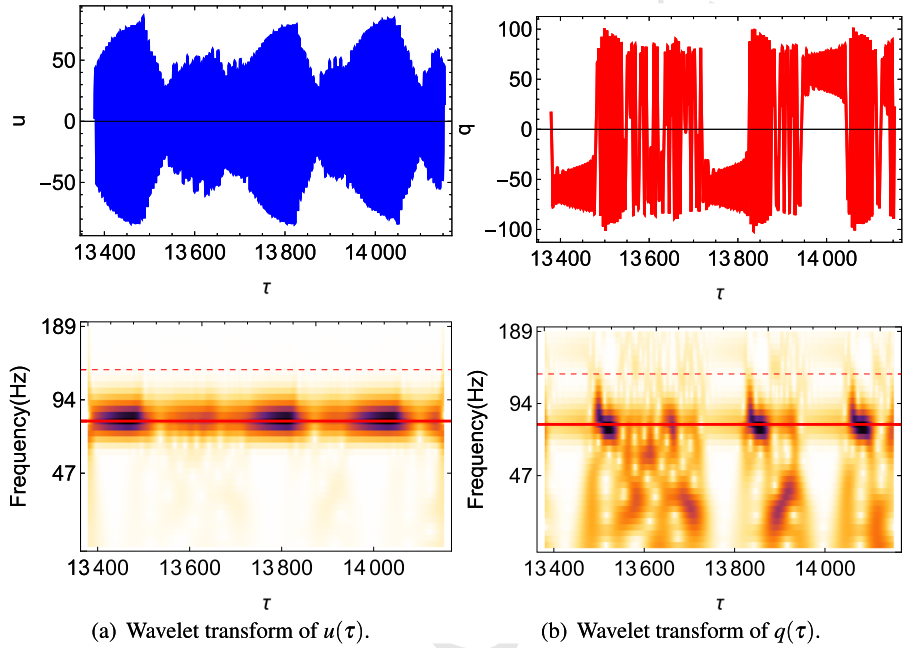


(a) Wavelet transform of $u(\tau)$. (b) Wavelet transform of $q(\tau)$.

**Fig. 22** Time response of the tube $u(\tau)$ and membrane $q(\tau)$ and wavelet transform for $k_l = -0.276$ at frequency $f = 80.2$ Hz and excitation amplitude $F = 4.4$

the characteristic curves show that the distance between the two intersection points becomes very small. At the limit, these two points merge, and the effects of softening and stiffening nonlinearity combine. This can explain the presence in the time response of simultaneous strongly modulated interwell and intrawell regimes.

In this zone, with the decrease in the linear stiffness value, an increase in the area is observed. Indeed, with this decrease, the natural frequency of the membrane becomes increasingly higher, leading to a corresponding amplitude of resonance capture becoming increasingly significant. Consequently, the activation threshold of energy pumping also becomes increasingly higher.

For the lowest values of linear stiffness, the area curve shows a constant variation. In this zone, the activation threshold of energy pumping becomes very high, and the range of the fixed excitation force for the calculation does not cover the energy pumping zone. Only the linear behavior zone observed before the energy pumping zone is detected.

### 6.3 Effectiveness of Bistable NES

Figure 23 shows the superposition of a ridge curve for a bistable membrane (red) with several ridge curves

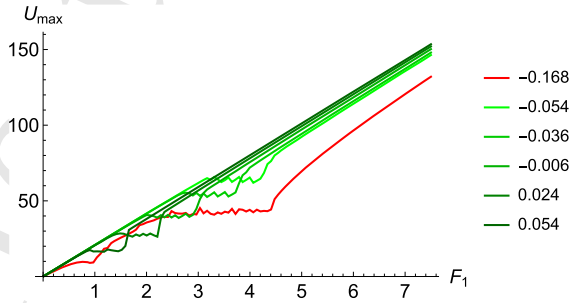


**Fig. 23** Ridge curve of a bistable membrane (red) and ridge curves of monostable membranes for the monostable minimum areas (green)

belonging to the monostable minimum plateau. This figure demonstrates that the use of a bistable membrane can significantly improve the system's behavior. The attenuation provided by a bistable membrane is greater than that obtained with the different optimal monostable membranes. Additionally, it is worth noting that the frequency range of energy pumping is wider when using the bistable NES, as clearly observed by comparing the frequency response surface for two linear stiffness values: $k_l = -0.276$ (Fig. 12a) and $k_l = -0.12$ (Fig. 17a).



Journal: 11071 MS: 10572 TYPESET DISK LE CP Disp.:2024/11/1 Pages: 20 Layout: Medium

## 7 Different membrane configurations

In this section, we present the results of our numerical optimization method for other membrane configurations. Figures 24 and 25 show the superposition of several curves representing the variation of the area given by the ridge curves as a function of the linear stiffness of the membrane for different membrane configurations. In Fig. 24, the membranes have the same thickness $h_m = 0.22 \cdot 10^{-3}$ m and three different rays $R_m = 4 \cdot 10^{-2}$ m, $R_m = 5 \cdot 10^{-2}$ m and $R_m = 6 \cdot 10^{-2}$ m. Whereas in Fig. 25, the membranes have the same radius $R_m = 5 \cdot 10^{-2}$ $m$ and different thicknesses $h_m = 0.22 \cdot 10^{-3}$ m, $h_m = 0.3 \cdot 10^{-3}$ m and $h_m = 0.3 \cdot 10^{-3}$ m. The dashed red line represents the boundary separating the monostable and bistable zones. In these figures, each area curve is associated with two vertical lines of the same color, representing the linear stiffness values at which the coupled natural frequency of the membrane becomes higher than that of the tube.

These two figures show that the variation of the area under the normalized ridge curve as a function of the membrane's linear stiffness exhibits the same pattern when using different membrane configurations. These results validate that the bistable minimum plateau is observed when the coupled natural frequency of the membrane becomes higher than that of the tube, and the monostable minimum plateau is observed when this frequency is lower than that of the tube.

The different curves show minimization plateaus at different area levels, widening unevenly over different linear stiffness ranges. In fact, as the radius of the membrane decreases, the minimization plateaus become wider, but corresponds to larger area values. So, for more effective attenuation with a membrane thickness of $h_m = 0.22 \cdot 10^{-3}$ m, it's better to use a membrane of radius $R_m = 6 \cdot 10^{-2}$ m with a pre-stress adjustment that corresponds, for the bistable membrane, to a linear stiffness value around $k_l = -0.14$ (which means buckling of $1.3 \cdot 10^{-2}$ m), and for the monostable membrane to a value in the range $[-0.056, 0.01]$ (where the membrane's coupled natural frequency can reach 82 Hz). Figure 25 shows that decreasing the membrane thickness improves the system attenuation in the zone of optimal behavior. As the membrane thickness decreases, the minimization plateaus narrow, while the area values become less important. So, for a membrane with radius $R_m = 5 \cdot 10^{-2}$ m, the optimum thickness among the three is $h_m = 0.22 \cdot 10^{-3}$ m with a pre-stress setting that corresponds, for the bistable membrane, to a linear stiffness value in the range $[-0.16, 0.22]$ (corresponding to a buckling range from $0.8 \cdot 10^{-2}$ to $10^{-2}$ m), and for the monostable membrane to a value in the range $[-0.056, 0.06]$ (where the membrane's coupled natural frequency can reach 64.8 Hz).

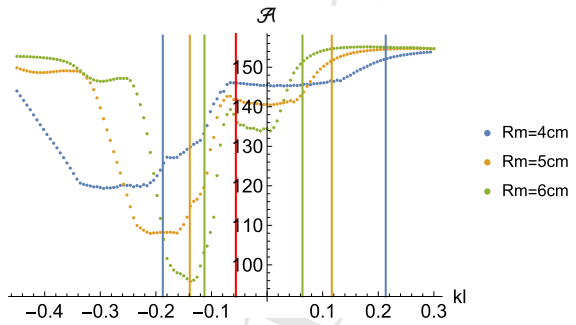


**Fig. 24** Normalized ridge curve area for different membrane radii as a function of linear stiffness. Membrane thickness $h_m = 0.22 \cdot 10^{-3}$ m

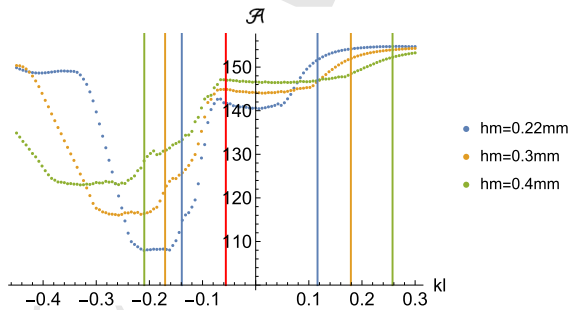


**Fig. 25** Normalized ridge curve area for different membrane thicknesses as a function of linear stiffness. Membrane radius $R_m = 5 \cdot 10^{-2}$ m

## 8 Conclusion

In this article, we demonstrate through a numerical approach that a solution based on a bistable membrane significantly improves the attenuation efficiency of NES membranes. We experimentally verify this result, despite the extremely simplified model describing the membrane. This method not only allows for comparing the performance of a bistable membrane with a monostable one but also for finding the optimal behavior for each type. This optimal behavior extends over a wide range of linear stiffnesses. This study shows the robustness of NES membranes, which, in the monostable or





Journal: 11071 MS: 10572 TYPESET DISK LE CP Disp.:2024/11/1 Pages: 20 Layout: Medium

bistable behavior zones, exhibit a wide range of optimal linear stiffnesses.

We describe a condition for getting the optimal behavior of the bistable NES: the natural frequency of the membrane must exceed that of the tube. In this case, the system presents two energy pumping zones in the excitation amplitude range. The pumping zone due to bistability is observed at low excitation amplitude, and characterized by a strongly modulated intrawell response. It is related to the softening nonlinearity of the bistable NES membrane which, when the natural frequency of the membrane is higher than that of the tube, induces a second resonance capture between the tube and the membrane.

By applying this numerical approach to six other membrane configurations, we confirm these results and show that increasing the radius of the membrane and decreasing its thickness can improve attenuation efficiency in the optimal linear stiffness range.

**Acknowledgements** The authors thank Tahar Fakhfakh and Mohamed Haddar from LA2MP, ENIS, Tunisia for their support.

**Author contributions** I.B. carried out most of the scientific work, under the supervision of R.C and P.-O. M. All authors contributed significantly to the manuscript. I.B. prepared the figures.

**Funding** The authors have not disclosed any funding.

**Data availability** Experimental data sets generated during the current study are available from the corresponding author on reasonable request.

**Declarations**

**Conflict of interest** The authors declare no conflict of interest.

## References


1. Geng, X.-F., Ding, H., Ji, J.-C., Wei, K.-X., Jing, X.-J., Chen, L.-Q.: A state-of-the-art review on the dynamic design of nonlinear energy sinks. Eng. Struct. **313**, 118228 (2024)
2. Cochelin, B., Herzog, P., Mattei, P.-O.: Experimental evidence of energy pumping in acoustics. Comptes Rendus Mécanique **334**(11), 639–644 (2006). https://doi.org/10.1016/j.crme.2006.08.005
3. Bellet, R.: Vers une nouvelle technique de contrôle passif du bruit: absorbeur dynamique non linéaire et pompage énergétique, Ph.D. thesis, Université de Provence-Aix-Marseille I (2010)
4. Bellet, R., Cochelin, B., Herzog, P., Mattei, P.-O.: Experimental study of targeted energy transfer from an acoustic system to a nonlinear membrane absorber. J. Sound Vib. **329**(14), 2768–2791 (2010). https://doi.org/10.1016/j.jsv.2010.01.029
5. Bellet, R., Cochelin, B., Côte, R., Mattei, P.-O.: Enhancing the dynamic range of targeted energy transfer in acoustics using several nonlinear membrane absorbers. J. Sound Vib. **331**(26), 5657–5668 (2012). https://doi.org/10.1016/j.jsv.2012.07.013
6. Mariani, R., Bellizzi, S., Cochelin, B., Herzog, P., Mattei, P.: Toward an adjustable nonlinear low frequency acoustic absorber. J. Sound Vib. **330**(22), 5245–5258 (2011). https://doi.org/10.1016/j.jsv.2011.03.034
7. Shao, J., Cochelin, B.: Theoretical and numerical study of targeted energy transfer inside an acoustic cavity by a nonlinear membrane absorber. Int. J. Non-Linear Mech. **64**, 85–92 (2014). https://doi.org/10.1016/j.ijnonlinmec.2014.04.008
8. Shao, J., Zeng, T., Wu, X.: Study of a nonlinear membrane absorber applied to 3d acoustic cavity for low frequency broadband noise control. Materials **12**(7), 1138 (2019). https://doi.org/10.3390/ma12071138
9. Shao, J., Luo, Q., Deng, G., Zeng, T., Yang, J., Wu, X., Jin, C.: Experimental study on influence of wall acoustic materials of 3d cavity for targeted energy transfer of a nonlinear membrane absorber. Appl. Acoust. **184**, 108342 (2021). https://doi.org/10.1016/j.apacoust.2021.108342
10. Al-Shudeifat, M.A.: Highly efficient nonlinear energy sink. Nonlinear Dyn. **76**(4), 1905–1920 (2014). https://doi.org/10.1007/s11071-014-1256-x
11. Manevitch, L.I., Sigalov, G., Romeo, F., Bergman, L.A., Vakakis, A.: Dynamics of a linear oscillator coupled to a bistable light attachment: analytical study. J. Appl. Mech. **81**(4), 041011 (2013). https://doi.org/10.1115/1.4025150
12. Romeo, F., Sigalov, G., Bergman, L.A., Vakakis, A.F.: Dynamics of a linear oscillator coupled to a bistable light attachment: numerical study. J. Comput. Nonlinear Dyn. (2014). https://doi.org/10.1115/1.4027224
13. Al-Shudeifat, M.A., Saeed, A.S.: Frequency-energy plot and targeted energy transfer analysis of coupled bistable nonlinear energy sink with linear oscillator. Nonlinear Dyn. **105**(4), 2877–2898 (2021). https://doi.org/10.1007/s11071-021-06802-8
14. Qiu, D., Li, T., Seguy, S., Paredes, M.: Efficient targeted energy transfer of bistable nonlinear energy sink: application to optimal design. Nonlinear Dyn. **92**(2), 443–461 (2018). https://doi.org/10.1007/s11071-018-4067-7
15. Johnson, D.R., Harne, R.L., Wang, K.W.: A disturbance cancellation perspective on vibration control using a bistable snap-through attachment. J. Vib. Acoust. (2014). https://doi.org/10.1115/1.4026673
16. Mattei, P.-O., Ponçot, R., Pachebat, M., Côte, R.: Nonlinear targeted energy transfer of two coupled cantilever beams coupled to a bistable light attachment. J. Sound Vib. **373**, 29–51 (2016). https://doi.org/10.1016/j.jsv.2016.03.008
17. Chiacchiari, S., Romeo, F., McFarland, D.M., Bergman, L.A., Vakakis, A.F.: Vibration-based energy harvesting via a bistable system: experimental study
18. Xia, Y., Ruzzene, M., Erturk, A.: Dramatic bandwidth enhancement in nonlinear metastructures via bistable attachments. Appl. Phys. Lett. **114**(9), 093501 (2019). https://doi.org/10.1063/1.5066329

19. Yao, H., Wang, Y., Xie, L., Wen, B.: Bi-stable buckled beam nonlinear energy sink applied to rotor system. Mech. Syst. Signal Process. **138**, 106546 (2020). https://doi.org/10.1016/j.ymssp.2019.106546
20. Benacchio, S., Malher, A., Boisson, J., Touzé, C.: Design of a magnetic vibration absorber with tunable stiffnesses. Nonlinear Dyn. **85**(2), 893–911 (2016). https://doi.org/10.1007/s11071-016-2731-3
21. Pennisi, G., Mann, B., Stephan, C., Michon, G.: Magnetic-strung nes with energy harvesting: Theoretical and experimental study of a new concept of nonlinear vibrations absorber. In *ECCOMAS Congress 2016* (2016)
22. Chen, Y.-Y., Qian, Z.-C., Zhao, W., Chang, C.-M.: A magnetic bi-stable nonlinear energy sink for structural seismic control. J. Sound Vib. **473**, 115233 (2020). https://doi.org/10.1016/j.jsv.2020.115233
23. Chen, Y., Su, W., Tesfamariam, S., Qian, Z., Zhao, W., Yang, Z., Zhou, F.: Experimental study of magnetic bistable nonlinear energy sink for structural seismic control. Soil Dyn. Earthq. Eng. **164**, 107572 (2023). https://doi.org/10.1016/j.soildyn.2022.107572
24. Iurasov, V.: Contrôle passif en vibroacoustique avec absorbeur dynamique bistable, Ph.D. thesis, Aix-Marseille (2018)
25. Vakakis, A.F., Paipetis, S.A.: The effect of a viscously damped dynamic absorber on a linear multi-degree-of-freedom system. J. Sound Vib. **105**(1), 49–60 (1986)
26. Huang, D., Li, R., Yang, G.: On the dynamic response regimes of a viscoelastic isolation system integrated with a nonlinear energy sink. Commun. Nonlinear Sci. Numer. Simulat. **79**, 104916 (2019)

Journal: 11071
Article:

# Author Query Form

**Please ensure you fill out your response to the queries raised below and return this form along with your corrections**

Dear Author

During the process of typesetting your article, the following queries have arisen. Please check your typeset proof carefully against the queries listed below and mark the necessary changes either directly on the proof/online grid or in the 'Author's response' area provided below

| Query | Details required | Author's response |
|---|---|---|
| 1. | Kindly check and confirm the inserted city name is correct for affiliation 1. | |
| 2. | A funding declaration is mandatory for publication in this journal. Please confirm that this declaration is accurate, or provide an alternative. | |